

Three-Dimensional Analytical Magnetic Resonance Imaging Phantom in the Fourier Domain

Cheng Guan Koay,* Joelle E. Sarlls, and Evren Özarslan

This work presents a basic framework for constructing a 3D analytical MRI phantom in the Fourier domain. In the image domain the phantom is modeled after the work of Kak and Roberts on a 3D version of the famous Shepp-Logan head phantom. This phantom consists of several ellipsoids of different sizes, orientations, locations, and signal intensities (or gray levels). It will be shown that the k -space signal derived from the phantom can be analytically expressed. As a consequence, it enables one to bypass the need for interpolation in the Fourier domain when testing image-reconstruction algorithms. More importantly, the proposed framework can serve as a benchmark for contrasting and comparing different image-reconstruction techniques in 3D MRI with a non-Cartesian k -space trajectory. The proposed framework can also be adapted for 3D MRI simulation studies in which the MRI parameters of interest may be introduced to the signal intensity from the ellipsoid. Magn Reson Med 58:430–436, 2007. Published 2007 Wiley-Liss, Inc.†

Key words: 3D analytical MRI phantom; 3D Fourier domain phantom; Fourier transform of an ellipsoid; MRI phantom; Shepp-Logan

A distinctive feature of magnetic resonance imaging (MRI) as compared to other tomographic imaging modalities, such as X-ray computed tomography (CT), single photon emission computed tomography (SPECT), and positron emission tomography (PET), is the data-acquisition space. In MRI it is known as “ k -space” and is a conjugate to the image space. There is inherent flexibility in encoding k -space, and many acquisition schemes have been proposed.

Interest in 3D MRI abounds due to the increase in signal-to-noise ratios (SNRs) provided by volume excitation, and the potential for isotropic voxel dimensions. In addition, there is a growing interest in 3D non-Cartesian k -space trajectories, which have an advantage in various applications, as can be gleaned from past and recent studies (1–15). However, to analyze the effectiveness of various 3D encoding schemes in simulation studies, a common and flexible analytical phantom in the Fourier domain is needed.

A simulated head section, which consists of several overlapping ellipses, was first proposed and used by Shepp and Logan (16) to compare techniques for reconstructing an image from projections through the image. In another important paper by Shepp (17), a 3D version of the Shepp-

Logan head phantom containing 17 ellipsoids annotated with relevant anatomical structures (e.g., nose, eyes, blood clots, ventricles, tumors, and many others) was proposed and used to investigate a numerical quadrature algorithm for MR image reconstruction from a set of parallel plane measurements. Later, a simplified version of this 3D head phantom was used by Kak and Roberts (18) and Kak and Slaney (19) to test cone beam reconstruction algorithms. In such studies, the advantage of using ellipses or ellipsoids is that the projection through these objects can be analytically expressed. In MRI simulation studies, the interest is on the k -space signal derived from these objects. In the 2D case the Fourier transform (FT) of an ellipse can be analytically expressed, as found in the work of Kak and Slaney (19) and Van de Walle et al. (20).

In this paper a common and flexible 3D analytical phantom in the Fourier domain is proposed. In the image domain the phantom is modeled after the one described in Refs. 18 and 19. It is shown that the 3D k -space signal derived from this phantom, which consists of several ellipsoids, can be analytically expressed. Specifically, the FT of an ellipsoid under a general nonsingular affine transformation is derived. The FT of an ellipsoid under a rigid transformation is then deduced. The specifics of the 3D phantom are outlined and the 3D phantom is used for testing purposes and illustrations. In the section on numerical testing, the numerical stability of the proposed framework is discussed. We conclude this paper by briefly discussing some potential applications.

MATERIALS AND METHODS

Basic Example of the FT of an Ellipsoid

In this subsection we discuss a simple problem whose solution will be the building block for our 3D phantom. Specifically, we are interested in the FT of an ellipsoid that is centered at the origin of the coordinate system and whose principal directions are aligned parallel to the coordinate axes (Fig. 1a).

Let the 3D FT of a function $g(x, y, z)$ be

$$G(k_x, k_y, k_z) \equiv \int_{-\infty}^{+\infty} \int_{-\infty}^{+\infty} \int_{-\infty}^{+\infty} g(x, y, z) e^{-i2\pi(k_x x + k_y y + k_z z)} dx dy dz, \quad [1]$$

and let $g(x, y, z)$ be defined as follows:

$$g(x, y, z) = \begin{cases} \rho & (x/a)^2 + (y/b)^2 + (z/c)^2 \leq 1 \\ 0 & (x/a)^2 + (y/b)^2 + (z/c)^2 > 1 \end{cases} \cdot \quad [2]$$

It is shown in Appendix A that the FT of $g(x, y, z)$ defined in Eq. [2] can be expressed as

National Institute of Child Health and Human Development, National Institutes of Health, Bethesda, Maryland, USA.

Grant sponsor: National Institute of Child Health and Human Development, NIH.

*Correspondence to: Cheng Guan Koay, National Institutes of Health, Building 13, Room 3W16, 13 South Drive, Bethesda, MD 20892. E-mail: guankoac@mail.nih.gov

Received 12 January 2007; revised 15 March 2007; accepted 8 April 2007.

DOI 10.1002/mrm.21292

Published online in Wiley InterScience (www.interscience.wiley.com).

Published 2007 Wiley-Liss, Inc. † This article is a US Government work and, as such, is in the public domain in the United States of America.

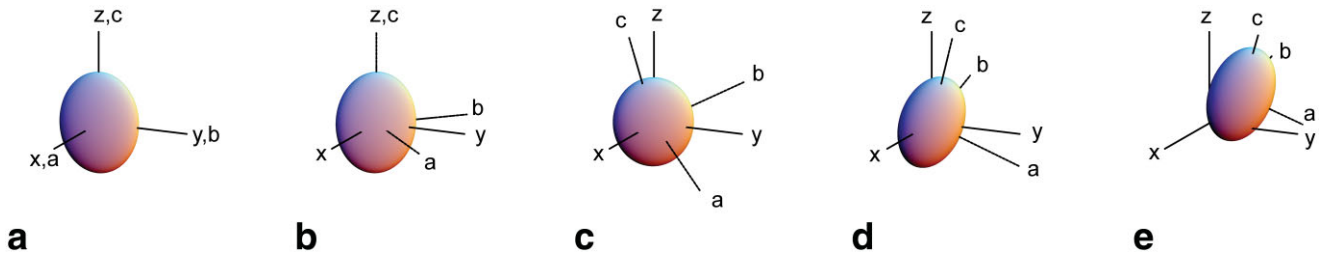


FIG. 1. **a**: An ellipsoid with its center located at the origin of the coordinate system and with its principal directions (a, b, c) aligned parallel to the coordinate axes (x, y, z). The effects of the rotation matrix defined as a series of counterclockwise rotations (about z by an angle $\psi = \pi/4$, then about y by an angle $\theta = \pi/6$, and finally about z by an angle $\phi = \pi/4$) are shown in **b**, **c**, and **d**, respectively. The effect of the displacement vector ($\delta_x = -0.25, \delta_y = 0.55, \delta_z = 0.55$) on the rotated ellipsoid is shown in **e**.

$$G(k_x, k_y, k_z) = \rho abc \left[\frac{\sin(2\pi K) - 2\pi K \cos(2\pi K)}{2\pi^2 K^3} \right], \quad [3]$$

where $K = ((ak_x)^2 + (bk_y)^2 + (ck_z)^2)^{1/2}$.

Before moving on to the general setting, it is instructive to reflect on two limiting cases. First, if all axes of the ellipsoid are of the same length, r , then it reduces to the FT of a sphere. Second, at the center of k -space, $G(0, 0, 0)$ is proportional to the volume of the ellipsoid. That is,

$$G(0, 0, 0) = \lim_{K \rightarrow 0} \rho abc \left[\frac{\sin(2\pi K) - 2\pi K \cos(2\pi K)}{2\pi^2 K^3} \right], \quad [4]$$

$$= \lim_{K \rightarrow 0} \rho abc \left[\frac{\frac{8}{3} \pi^3 K^3 - \frac{16}{15} \pi^5 K^5 + \dots}{2\pi^2 K^3} \right] = \rho \frac{4}{3} \pi abc. \quad [5]$$

In Eq. [5] the denominator inside the bracket was expanded in terms of Taylor series about $K = 0$. In the case of a sphere, $G(0, 0, 0) = \rho \frac{4}{3} \pi r^3$, which is a product of ρ and the volume of a sphere of radius r . It should be noted here that the formula for the FT of a sphere can be found in a previous work by Bracewell (21).

FT of an Ellipsoid Under a Constant Nonsingular Affine Transformation

The general case is no more difficult than the example discussed above. However, the key concept in this subsection is that of a coordinate transformation. That is, the function g is now a function of a new set of variables (p_x, p_y, p_z), and these new variables are themselves functions of the original coordinates.

Let the 3D FT of a function $g(p_x, p_y, p_z)$ be

$$G(k_x, k_y, k_z) \equiv \int_{-\infty}^{+\infty} \int_{-\infty}^{+\infty} \int_{-\infty}^{+\infty} g(p_x, p_y, p_z) e^{-i2\pi(k_x x + k_y y + k_z z)} dx dy dz, \quad [6]$$

where p_x, p_y , and p_z are functions of x, y and z . Specifically, we have the following expressions:

$$g(p_x, p_y, p_z) = \begin{cases} \rho & (p_x/a)^2 + (p_y/b)^2 + (p_z/c)^2 \leq 1 \\ 0 & (p_x/a)^2 + (p_y/b)^2 + (p_z/c)^2 > 1 \end{cases}, \quad [7]$$

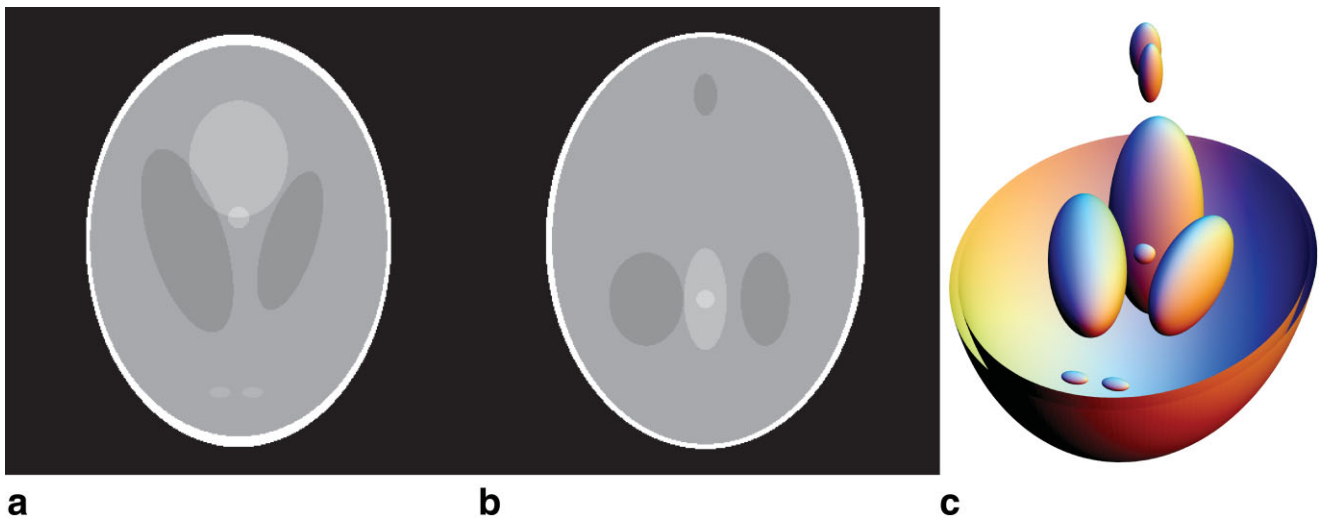


FIG. 2. **a**: An x - y plane cross section of the 3D version of the Shepp-Logan head phantom at $z = -0.25$. **b**: An x - z plane cross section of the 3D version of the Shepp-Logan head phantom at $y = 0.125$. **c**: A 3D rendering of the 3D version of the Shepp-Logan head phantom. The top portion of the skull is removed to show the smaller ellipsoids.

and

$$\begin{pmatrix} p_x \\ p_y \\ p_z \end{pmatrix} = \mathbf{A}^{-1} \left(\begin{pmatrix} x \\ y \\ z \end{pmatrix} - \begin{pmatrix} \delta_x \\ \delta_y \\ \delta_z \end{pmatrix} \right), \quad [8]$$

where \mathbf{A} is a constant nonsingular 3×3 matrix, and $\boldsymbol{\delta} = [\delta_x, \delta_y, \delta_z]^T$ is a constant translation or displacement vector. The vector or matrix transposition is denoted by a superscript T . Rewriting x , y , and z in terms of p_x , p_y , and p_z , Eq. [8] is transformed to the following expression:

$$\mathbf{r} = \mathbf{A}\mathbf{p} + \boldsymbol{\delta}, \quad [9]$$

where $\mathbf{r} = [x, y, z]^T$, and $\mathbf{p} = [p_x, p_y, p_z]^T$.

Another means of expressing the integral in Eq. [6] is to state the region of integration, which is written as

$$G(k_x, k_y, k_z) = \rho \iiint_R e^{-i2\pi(k_x x + k_y y + k_z z)} dx dy dz, \quad [10]$$

where R is the ellipsoidal region defined by $(p_x/a)^2 + (p_y/b)^2 + (p_z/c)^2 \leq 1$.

Performing a change of variables from (x, y, z) to (p_x, p_y, p_z) , the integral above takes the following form:

$$G(k_x, k_y, k_z) = \rho \iiint_R e^{-i2\pi\mathbf{k}^T \cdot \mathbf{r}} |\det(\mathbf{A})| dp_x dp_y dp_z, \quad [11]$$

where $\mathbf{k} = [k_x, k_y, k_z]^T$, and $|\det(\mathbf{A})|$ denotes the absolute value of the determinant of \mathbf{A} . Substituting Eq. [9] into Eq. [11], this yields

$$\begin{aligned} G(k_x, k_y, k_z) &= \rho \iiint_R e^{-i2\pi\mathbf{k}^T(\mathbf{A}\mathbf{p} + \boldsymbol{\delta})} |\det(\mathbf{A})| dp_x dp_y dp_z, \\ &= \rho |\det(\mathbf{A})| e^{-i2\pi\mathbf{k}^T \boldsymbol{\delta}} \iiint_R e^{-i2\pi(\mathbf{A}^T \mathbf{k})^T \mathbf{p}} \\ &\quad \times dp_x dp_y dp_z. \end{aligned} \quad [12]$$

By defining $\tilde{\mathbf{k}} = \mathbf{A}^T \mathbf{k}$, Eq. [12] reduces to

$$G(k_x, k_y, k_z) = \rho |\det(\mathbf{A})| e^{-i2\pi\mathbf{k}^T \boldsymbol{\delta}} \iiint_R e^{-i2\pi\tilde{\mathbf{k}}^T \mathbf{p}} dp_x dp_y dp_z. \quad [13]$$

Note that the integral in Eq. [13] is exactly the FT of an ellipsoid under the condition discussed in previous subsection if we replace the vector \mathbf{k} in Eq. [3] by the vector $\tilde{\mathbf{k}}$ in Eq. [13]. Therefore, the FT of an ellipsoid under the affine transformation discussed here is

$$\begin{aligned} G(k_x, k_y, k_z) \\ &= \rho abc |\det(\mathbf{A})| e^{-i2\pi\mathbf{k}^T \boldsymbol{\delta}} \left[\frac{\sin(2\pi K) - 2\pi K \cos(2\pi K)}{2\pi^2 K^3} \right] \end{aligned} \quad [14]$$

where $K = ((a\tilde{k}_x)^2 + (b\tilde{k}_y)^2 + (c\tilde{k}_z)^2)^{1/2}$ and $\tilde{\mathbf{k}} = \mathbf{A}^T \mathbf{k}$.

FT of an Ellipsoid Under a Rigid-Body Transformation

In this case the general nonsingular 3×3 matrix \mathbf{A} is replaced by a proper rotation matrix, \mathbf{R} , (Fig. 1b–e). This substitution yields the following properties: $\det(\mathbf{R}) = 1$, $\mathbf{r} = \mathbf{R}\mathbf{p} + \boldsymbol{\delta}$, and $\mathbf{p} = \mathbf{R}^T(\mathbf{r} - \boldsymbol{\delta})$. Based on these properties, the expression of $G(k_x, k_y, k_z)$ under a rigid-body transformation can further be simplified to:

$$G(k_x, k_y, k_z) = \rho abc e^{-i2\pi\mathbf{k}^T \boldsymbol{\delta}} \left[\frac{\sin(2\pi K) - 2\pi K \cos(2\pi K)}{2\pi^2 K^3} \right], \quad [15]$$

where $K = ((a\tilde{k}_x)^2 + (b\tilde{k}_y)^2 + (c\tilde{k}_z)^2)^{1/2}$ and $\tilde{\mathbf{k}} = \mathbf{R}^T \mathbf{k}$.

3D Phantom

The 3D version of the Shepp-Logan head phantom used in Refs. 18 and 19 was adapted for testing purposes. The specification of this head phantom can also be found in Ref. 19. For convenience, we provide here a slightly modified version of the 3D head phantom of Refs. 18 and 19. Before going into the specifics of the phantom, it should be noted that the convention used in defining the rotation in terms of the Euler angles is $\mathbf{R} = \mathbf{R}_z(\phi)\mathbf{R}_y(\theta)\mathbf{R}_z(\psi)$, where $\mathbf{R}_z(\phi)$, $\mathbf{R}_y(\theta)$, and $\mathbf{R}_z(\psi)$ are defined in Appendix B.

Table 1 shows the exact specification for the head phantom of Refs. 18 and 19 except for the last column, where the signal intensities are slightly changed for better visual perception since our interest is in numerical testing and not in simulating tissue properties (16,17). Figure 2a shows a horizontal cross section of the head phantom at $z = -0.25$, whereas Fig. 2b shows a vertical cross section of the head phantom at $y = 0.125$. Figure 2c is a 3D rendering of the head phantom after a virtual hemicraniectomy procedure.

Numerical Test

The goal of the numerical testing was to show that an image of the 3D head phantom can be reconstructed from the k -space signals calculated by the expression in Eq. [15]. As an example, the expression in Eq. [15] was evaluated numerically for a finite number of Cartesian points ($128 \times 128 \times 128$) and for all the ellipsoids associated with the 3D head phantom as described in Table 1. The increment in k -space is 0.5 and is the same for each k -space dimension; in other words, each dimension of the k -space is sampled, inclusive of the two end points, from -31.5 to 32 with a step size of 0.5. A slice from the image of the 3D head phantom reconstructed from the k -space is shown in Fig. 3a. This figure is the Fourier-reconstructed image of Fig. 2a. Figure 3b is a plot of both the Fourier-reconstructed intensity profile (solid line) and the true intensity

Table 1
Specification for the 3-D Head Phantom*

| Ellipsoid | Coordinates of the center or $(\delta_x, \delta_y, \delta_z)$ | Axis lengths (a,b,c) | Euler angle ϕ (radian) | Gray level ρ |
|-----------|---|------------------------|-----------------------------|-------------------|
| a | (0,0,0) | (0.69,0.92,0.9) | 0 | 2.0 |
| b | (0,0,0) | (0.6624,0.874,0.88) | 0 | -0.8 |
| c | (-0.22,0,-0.25) | (0.41,0.16,0.21) | $3\pi/5$ | -0.2 |
| d | (0.22,0,-0.25) | (0.31,0.11,0.22) | $2\pi/5$ | -0.2 |
| e | (0,0.35,-0.25) | (0.21,0.25,0.5) | 0 | 0.2 |
| f | (0,0.1,-0.25) | (0.046,0.046,0.046) | 0 | 0.2 |
| g | (-0.08,-0.65,-0.25) | (0.046,0.023,0.02) | 0 | 0.1 |
| h | (0.06,-0.65,-0.25) | (0.046,0.023,0.02) | $\pi/2$ | 0.1 |
| i | (0.06,-0.105,0.625) | (0.056,0.04,0.1) | $\pi/2$ | 0.2 |
| j | (0,0.1,0.625) | (0.056,0.056,0.1) | 0 | -0.2 |

*These parameters are exactly the same (except for the last column) as used by Kak and Roberts (18) and Kak and Slaney (19). The parameters are reinterpreted in terms of the convention used in this paper. For example, the coordinates of the center of an ellipsoid would be the translation vector, $\delta = [\delta_x, \delta_y, \delta_z]^T$ and the angle is reinterpreted as one of the Euler angles. In this 3-D phantom, the other two Euler angles, θ and ψ , are set to zero.

profile (dashed line) along the horizontal line depicted in Fig. 3a.

Based on our numerical test, the expression

$$\frac{\sin(2\pi K) - 2\pi K \cos(2\pi K)}{2\pi^2 K^3},$$

which is common to all three equations (Eqs. [4], [14], and [15]), is not numerically stable around $K = 0$. This issue can be resolved by using the Taylor expansion: the first three nonzero terms in the Taylor series are used to compute the k -space signal instead of the expression above if K is less than some small numerical value (say, 0.002). The three-term expression is given by:

$$\frac{4}{3} \pi - \frac{8}{15} \pi^3 K^2 + \frac{8}{105} \pi^5 K^4.$$

DISCUSSION

Here we outline the main findings of this work. As a tool for MRI simulation and phantom studies, the proposed framework has several desirable features, namely, that the FT of an ellipsoid under a nonsingular affine transformation can be analytically expressed, and that the proposed framework can serve as a benchmark for comparing differ-

ent image-reconstruction techniques in 3D MRI with a non-Cartesian k -space trajectory. This framework will be most convenient and helpful to researchers whose interest is in 3D MRI with a non-Cartesian k -space trajectory because the expression for the k -space signal is analytically expressed and can be evaluated in any coordinate system by a suitable coordinate transformation. In other words, this framework enables one to bypass k -space interpolation. As a consequence, this framework provides a means of teasing apart two of the key factors affecting the quality of a reconstructed image (i.e., the k -space interpolation and the image-reconstruction method (17)) so that a more objective comparison of different k -space encoding schemes can be achieved. Further, this framework can be used to test 3D k -space resampling and gridding techniques (20,24–27).

Another important aspect of this framework is that it can be used as a platform for testing algorithms that deal with motion correction, distortion correction, and image registration in 3D MRI. Suppose there are many tiny, nonintersecting ellipsoids located throughout the whole imaging volume such that each ellipsoid is affected by a *local* affine transformation. In this example, we can infer that local distortion modeled by an affine transformation in an image space will affect the k -space globally. In light of this example, it may be said that the proposed framework may be

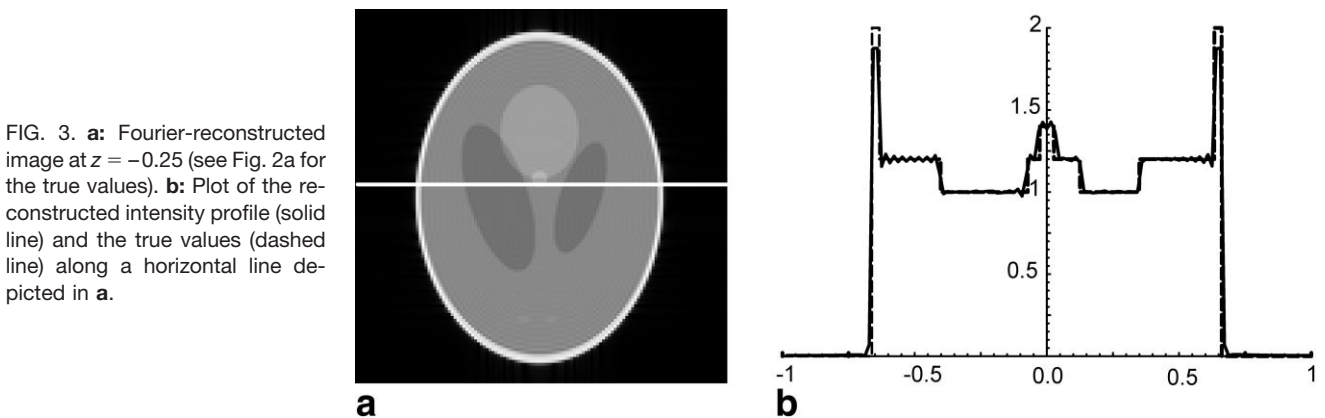


FIG. 3. **a:** Fourier-reconstructed image at $z = -0.25$ (see Fig. 2a for the true values). **b:** Plot of the reconstructed intensity profile (solid line) and the true values (dashed line) along a horizontal line depicted in **a**.

useful for understanding and testing methods in image registration, distortion correction, and motion correction.

As mentioned above, a distinctive feature of MRI compared to other imaging modalities is the fact that data are acquired directly in the Fourier domain. However, the expansive utility of MRI is due to the multitude of its contrast mechanisms. The present framework can also allow for realistic 3D simulation studies since the image-space signal intensity within each ellipsoid can be modeled as a function of MRI parameters such as the proton density, longitudinal relaxation time (T1), transverse relaxation time (T2), diffusion coefficient, diffusion anisotropy, and diffusion tensor (28–30). In addition to modeling the signal intensity of the ellipsoid, one can also model the principal axes of the ellipsoid so that these axes will be functions of time. For example, an ellipsoid can be programmed to mimic a series of cardiac contractions. Finally, this framework will also be useful for functional MRI (fMRI) simulation studies, and particularly for studies comparing the relative merits of various methods of fMRI analysis.

The analytical expression for the 2D FT of an ellipse under planar rotation and translation can be found in Refs. 19 and 20. Based on the approach presented here, it is easy to see that this result can be extended to a more general transformation, namely, the 2D affine transformation. For completeness, the expression of the FT of an ellipse under a general nonsingular affine transformation is provided in Appendix C together with a brief discussion on the numerical stability of the relevant expression (numerical stability was not discussed in Refs. 19 and 20). The notations used in Appendix C are similar to those presented in Materials and Methods.

CONCLUSIONS

This paper provides a basic framework for constructing a 3D analytical MRI phantom in the Fourier domain that can be used to compare different non-Cartesian encoding schemes and reconstruction methods. Most importantly, the k -space signal for the 3D phantom can be evaluated analytically and sampled according to any chosen k -space trajectory or encoding scheme. It can also be adapted to simulate tissue with realistic relaxation and diffusion properties.

ACKNOWLEDGMENT

C.G.K. dedicates this work to Elie Koay.

APPENDIX A

In this appendix we derive the FT of an ellipsoid under the simplest condition discussed in the “Basic Example of the FT of an Ellipsoid” section above.

From Eqs. [1] and [2] we have

$$G(k_x, k_y, k_z) \equiv \int_{-\infty}^{+\infty} \int_{-\infty}^{+\infty} \int_{-\infty}^{+\infty} \times g(x, y, z) e^{-i2\pi(k_x x + k_y y + k_z z)} dx dy dz \quad [A1]$$

$$g(x, y, z) = \begin{cases} \rho & (x/a)^2 + (y/b)^2 + (z/c)^2 \leq 1 \\ 0 & (x/a)^2 + (y/b)^2 + (z/c)^2 > 1 \end{cases} \quad [A2]$$

Then, Eq. [A1] can be rewritten as

$$G(k_x, k_y, k_z) \equiv \rho \iiint_{R_1} e^{-i2\pi(k_x x + k_y y + k_z z)} dx dy dz \quad [A3]$$

where R_1 is the ellipsoidal region defined by $(x/a)^2 + (y/b)^2 + (z/c)^2 \leq 1$.

By a change of variables,

$$x = a\xi, y = b\eta, \text{ and } z = c\zeta, \quad [A4]$$

The integral can be expressed in the new coordinate system (ξ, η, ζ) as follows:

$$G(\tilde{k}_x, \tilde{k}_y, \tilde{k}_z) \equiv \rho abc \iiint_{R_2} e^{-i2\pi(\tilde{k}_x \xi + \tilde{k}_y \eta + \tilde{k}_z \zeta)} d\xi d\eta d\zeta \quad [A5]$$

where R_2 is the spherical region defined by $\xi^2 + \eta^2 + \zeta^2 \leq 1$ and $\tilde{k}_x = ak_x$, $\tilde{k}_y = bk_y$, and $\tilde{k}_z = ck_z$. Further simplification can be achieved by another change of variables from (ξ, η, ζ) to the spherical coordinates, (r, θ_1, ϕ_1) :

$$\xi = r \sin(\theta_1) \cos(\phi_1), \eta = r \sin(\theta_1) \sin(\phi_1), \text{ and } \zeta = r \cos(\theta_1). \quad [A6]$$

By defining $\tilde{\mathbf{k}} \equiv [\tilde{k}_x, \tilde{k}_y, \tilde{k}_z]^T = [\tilde{k} \sin(\theta_2) \cos(\phi_2), \tilde{k} \sin(\theta_2) \sin(\phi_2), \tilde{k} \cos(\theta_2)]^T$ and $\mathbf{r} = [r \sin(\theta_1) \cos(\phi_1), r \sin(\theta_1) \sin(\phi_1), r \cos(\theta_1)]^T$, the integral in Eq. [A5] can be reduced to

$$G(\tilde{\mathbf{k}}) \equiv \rho abc \int_0^{2\pi} \int_0^\pi \int_0^1 e^{-i2\pi \tilde{\mathbf{k}}^T \mathbf{r}} \sin(\theta_1) r^2 dr d\theta_1 d\phi_1 \quad [A7]$$

$$= \rho abc \int_0^{2\pi} \int_0^\pi \int_0^1 e^{-i2\pi \tilde{k} r \cos(\gamma)} \sin(\theta_1) r^2 dr d\theta_1 d\phi_1 \quad [A8]$$

where $\cos(\gamma) = \cos(\theta_1) \cos(\theta_2) + \sin(\theta_1) \sin(\theta_2) \cos(\phi_1 - \phi_2)$ (22).

A useful integral representation of elementary spherical wave functions is given by (23):

$$j_n(2\pi \tilde{k} r) P_n(\cos(\theta_2)) = \frac{(-j)^n}{4\pi} \int_0^{2\pi} \int_0^{2\pi} e^{-i2\pi \tilde{k} r \cos(\gamma)} P_n(\cos(\theta_1)) \sin(\theta_1) d\theta_1 d\phi_1 \quad [A9]$$

where j_n is the spherical Bessel function of order n and P_n is the Legendre polynomial of order n .

Using the above relation for the case $n = 0$, Eq. [A9] reduces to

$$j_0(2\pi\tilde{k}r) = \frac{1}{4\pi} \int_0^{2\pi} \int_0^\pi e^{-i2\pi\tilde{k}r \cos(\gamma)} \sin(\theta_1) d\theta_1 d\phi_1. \quad [\text{A10}]$$

It is obvious then that Eq. [A8] can be simplified to:

$$G(\tilde{\mathbf{k}}) = 4\pi\rho abc \int_0^1 j_0(2\pi\tilde{k}r) r^2 dr \quad [\text{A11}]$$

Since $j_0(x) = \sin(x)/x$, Eq. [A11] can further be reduced to

$$G(\tilde{\mathbf{k}}) = \frac{4\pi\rho abc}{2\pi\tilde{k}} \int_0^1 \sin(2\pi\tilde{k}r) r dr, \quad [\text{A12}]$$

$$= \frac{2\rho abc}{\tilde{k}} \left(\frac{\sin(2\pi\tilde{k}) - 2\pi\tilde{k} \cos(2\pi\tilde{k})}{(2\pi\tilde{k})^2} \right), \quad [\text{A13}]$$

$$= \rho abc \left(\frac{\sin(2\pi\tilde{k}) - 2\pi\tilde{k} \cos(2\pi\tilde{k})}{2\pi^2\tilde{k}^3} \right). \quad [\text{A14}]$$

As a reminder, we define $K \equiv \tilde{k}$ in the main text, and $\tilde{k} = (\tilde{k}_x^2 + \tilde{k}_y^2 + \tilde{k}_z^2)^{1/2} = ((ak_x)^2 + (bk_y)^2 + (ck_z)^2)^{1/2}$ as defined in this appendix. Therefore, the final expression is

$$G(k_x, k_y, k_z) \equiv \rho abc \left(\frac{\sin(2\pi K) - 2\pi K \cos(2\pi K)}{2\pi^2 K^3} \right) \quad [\text{A15}]$$

where $K \equiv ((ak_x)^2 + (bk_y)^2 + (ck_z)^2)^{1/2}$.

APPENDIX B

The rotation matrices $\mathbf{R}_x(\Omega)$, $\mathbf{R}_y(\Omega)$ and $\mathbf{R}_z(\Omega)$ represent rotations through angle Ω around the x -, y -, and z -axes, respectively, and are defined as follows:

$$\mathbf{R}_x(\Omega) = \begin{pmatrix} 1 & 0 & 0 \\ 0 & \cos(\Omega) & -\sin(\Omega) \\ 0 & \sin(\Omega) & \cos(\Omega) \end{pmatrix},$$

$$\mathbf{R}_y(\Omega) = \begin{pmatrix} \cos(\Omega) & 0 & \sin(\Omega) \\ 0 & 1 & 0 \\ -\sin(\Omega) & 0 & \cos(\Omega) \end{pmatrix}, \text{ and}$$

$$\mathbf{R}_z(\Omega) = \begin{pmatrix} \cos(\Omega) & -\sin(\Omega) & 0 \\ \sin(\Omega) & \cos(\Omega) & 0 \\ 0 & 0 & 1 \end{pmatrix}.$$

APPENDIX C

In this appendix we do not derive the FT of an ellipse under an affine transformation, but provide the expression using the notations presented in the text.

Suppose the 2D FT of $g(x, y)$ is $G(k_x, k_y) \equiv \int_{-\infty}^{+\infty} \int_{-\infty}^{+\infty} g(x, y) e^{-i2\pi(k_x x + k_y y)} dx dy$. The FT of an ellipse under a 2D affine transformation is given by

$$G(k_x, k_y) \equiv \int_{-\infty}^{+\infty} \int_{-\infty}^{+\infty} g(p_x, p_y) e^{-i2\pi(k_x p_x + k_y p_y)} dx dy, \quad [\text{C1}]$$

where p_x , and p_y are functions of x , and y , and $g(p_x, p_y)$ is defined by:

$$g(p_x, p_y) = \begin{cases} \rho & (p_x/a)^2 + (p_y/b)^2 \leq 1 \\ 0 & (p_x/a)^2 + (p_y/b)^2 > 1 \end{cases},$$

and

$$\begin{pmatrix} p_x \\ p_y \end{pmatrix} = \mathbf{A}^{-1} \left(\begin{pmatrix} x \\ y \end{pmatrix} - \begin{pmatrix} \delta_x \\ \delta_y \end{pmatrix} \right),$$

where \mathbf{A} is a 2×2 nonsingular matrix. The final result of Eq. [C1] is

$$G(k_x, k_y) \equiv \rho\pi ab |\det(\mathbf{A})| e^{-2\pi i \mathbf{k}^T \cdot \delta} \left(\frac{J_1(2\pi K)}{\pi K} \right) \quad [\text{C2}]$$

where J_1 is a Bessel function of the first kind of first order, $K = ((a\tilde{k}_x)^2 + (b\tilde{k}_y)^2)^{1/2}$ and $\begin{pmatrix} \tilde{k}_x \\ \tilde{k}_y \end{pmatrix} = \mathbf{A}^T \begin{pmatrix} k_x \\ k_y \end{pmatrix}$. Equation [C2] is not numerically stable around $K = 0$, but this issue can be resolved using a three-term Taylor series of $(J_1(2\pi K)/\pi K)$ when $K \leq 0.001$, which is given by

$$\left(\frac{J_1(2\pi K)}{\pi K} \right) \approx 1 - \frac{(\pi K)^2}{2} + \frac{(\pi K)^4}{12}. \quad [\text{C3}]$$

REFERENCES

- Lai CM, Lauterbur P. True three-dimensional image reconstruction by nuclear magnetic resonance zeugmatography. *Phys Med Biol* 1981;26: 851–856.
- Meyer C, Hu B, Nishimura D, Macovski A. Fast spiral coronary artery imaging. *Magn Reson Med* 1992;28:202–213.
- Glover GH, Pauly JM, Bradshaw KM. Boron-11 imaging with a three-dimensional reconstruction method. *J Magn Reson Imaging* 1992;2:47–52.
- Irrazabal P, Nishimura DG. Fast three dimensional magnetic resonance imaging. *Magn Reson Med* 1995;33:656–662.
- Shattuck MD, Gewalt SL, Glover GH, Hedlund LW, Johnson GA. MR microimaging of the lung using volume projection encoding. *Magn Reson Med* 1997;38:938–942.
- Irrazabal P, Santos JM, Guarini M, Nishimura D. Flow properties of fast three-dimensional sequences for MR angiography. *Magn Reson Imaging* 1999;17:1469–1479.
- Thekens DR, Irrazabal P, Sachs TS, Meyer CH, Nishimura DG. Fast magnetic resonance coronary angiography with a three-dimensional stack of spirals trajectory. *Magn Reson Med* 1999;41:1170–1179.
- Tsai CM, Nishimura DG. Reduced aliasing artifacts using variable-density k-space sampling trajectories. *Magn Reson Med* 2000;43:452–458.
- Barger AV, Block WF, Toropov Y, Grist TM, Mistretta CA. Time-resolved contrast-enhanced imaging with isotropic resolution and broad coverage using an undersampled 3D projection trajectory. *Magn Reson Med* 2002;48:297–305.
- Lee JH, Hargreaves BA, Hu BS, Nishimura DG. Fast 3D imaging using variable-density spiral trajectories with applications to limb perfusion. *Magn Reson Med* 2003;50:1276–1285.
- Spiniak J, Guesalaga A, Mir R, Guarini M, Irrazabal P. Undersampling k-space using fast progressive 3D trajectories. *Magn Reson Med* 2005; 54:886–892.
- Gurney PT, Hargreaves BA, Nishimura DG. Design and analysis of a practical 3D cones trajectory. *Magn Reson Med* 2006;55:575–582.

13. Rahmer J, Börnert P, Groen J, Bos C. Three dimensional radial ultra-short echo-time imaging with T2 adapted sampling. *Magn Reson Med* 2006;55:1075–1082.
14. Shu Y, Riederer SJ, Bernstein MA. Three-dimensional MRI with an undersampled spherical shells trajectory. *Magn Reson Med* 2006;56:553–562.
15. Sarlls JE, Newbould RD, Moore S, Altbach MI, Gmitro AF, Trouard TP. Three dimensional isotropic DWMRI in a single radial-FSE scan. In: Proceedings of the 13th Annual Meeting of ISMRM, Miami Beach, FL, USA, 2005 (Abstract 1287).
16. Shepp LA, Logan BF. The Fourier reconstruction of a head section. *IEEE Trans Nucl Sci* 1974;NS-21:21–43.
17. Shepp LA. Computerized tomography and nuclear magnetic resonance. *J Comput Assist Tomogr* 1980;4:94–107.
18. Kak AC, Roberts B. Image reconstruction from projections. In: Young TY, Fu KS, editors. *Handbook of pattern recognition and image processing*. New York: Academic Press; 1986.
19. Kak AC, Slaney M. *Principles of computerized tomographic imaging*. IEEE Press, New York, 1988.
20. Van de Walle R, Barrett HH, Myers KJ, Altbach MI, Desplanques B, Gmitro AF, Cornelis J, Lemahieu I. Reconstruction of MR images from data acquired on a general nonregular grid by pseudoinverse calculation. *IEEE Trans Med Imaging* 2000;19:1160–1167.
21. Bracewell RN. *The Fourier transform and its applications*. 2nd rev. ed. New York: McGraw-Hill; 1986. p 253.
22. Arfken GB, Weber HJ. *Mathematical methods for physicists*. 5th ed. New York: Academic Press; 2001. p 796.
23. Stratton JA. *Electromagnetic theory*. New York: McGraw-Hill; 1941. p 410.
24. Jackson J, Meyer C, Nishimura D, Mocoovski A. Selection of a convolution function for Fourier inversion using gridding. *IEEE Trans Med Imaging* 1991;10:473–478.
25. Pipe JG, Menon P. Sampling density compensation in MRI: rationale and an iterative numerical solution. *Magn Reson Med* 1999;41:179–186.
26. Rasche V, Proska R, Sinkus R, Bornert P, Eggers H. Resampling of data between arbitrary grids using convolution interpolation. *IEEE Trans Med Imaging* 1999;18:385–392.
27. Sedarat H, Nishimura DG. On optimality of the gridding reconstruction algorithm. *IEEE Trans Med Imaging* 2000;19:306–317.
28. Basser PJ, Mattiello J, LeBihan D. MR diffusion tensor and imaging. *Biophys J* 1994;66:259–267.
29. Basser PJ. Inferring microstructural features and the physiological state of tissues from diffusion-weighted images. *NMR Biomed* 1995;8:333–344.
30. Pierpaoli C, Basser PJ. Toward a quantitative assessment of diffusion anisotropy. *Magn Reson Med* 1996;36:893–906.